OpenIllumination: A Multi-Illumination Dataset for Inverse Rendering Evaluation on Real Objects

Isabella Liu[1*], **Linghao Chen**[1,2*], **Ziyang Fu**[1], **Liwen Wu**[1], **Haian Jin**[2], **Zhong Li**[3],

Chin Ming Ryan Wong[3], **Yi Xu**[3], **Ravi Ramamoorthi**[1], **Zexiang Xu**[4], **Hao Su**[1]

[1]UC San Diego, [2]Zhejiang University, [3] OPPO US Research Center,
[4] Adobe Research, [*]Equal Contribution,
`{lal005,lic032,zifu,liw026,ravi,haosu}@ucsd.edu`
`{chenlinghao,haian}@zju.edu.cn`
`zexiangxu@gmail.com`
`{zhong.li,ryan.wong,yi.xu}@oppo.com`

Abstract

We introduce OpenIllumination, a real-world dataset containing over 108K images of 64 objects with diverse materials, captured under 72 camera views and a large number of different illuminations. For each image in the dataset, we provide accurate camera parameters, illumination ground truth, and foreground segmentation masks. Our dataset enables the quantitative evaluation of most inverse rendering and material decomposition methods for real objects. We examine several state-of-the-art inverse rendering methods on our dataset and compare their performances. The dataset and code can be found on the project page: https://oppo-us-research.github.io/OpenIllumination.

1 Introduction

Recovering object geometry, material, and lighting from images is a crucial task for various applications, such as image relighting and view synthesis. While recent works have shown promising results by using a differentiable renderer to optimize these parameters using the photometric loss [51, 53, 52, 20, 32], they can only perform a quantitative evaluation on synthetic datasets since it is easy to obtain ground-truth information. In contrast, they can only show qualitative results instead of providing quantitative evaluations in real scenes.

Nevertheless, it is crucial to acknowledge the inherent gap between synthetic and real-world data, for real-world scenes exhibit intricate complexities, such as natural illuminations, diverse materials, and complex geometry, which may present challenges that synthetic data fails to model accurately. Consequently, it becomes imperative to complement synthetic evaluation with real-world data to validate and assess the ability of inverse rendering algorithms in practical settings.

It is highly challenging to capture real objects in practice. A common approach to capturing real-world data is using a handheld camera [20, 53]. Unfortunately, this approach frequently introduces the occlusion of ambient light by photographers and cameras, consequently resulting in different illuminations for each photograph. Such discrepancies are unreasonable for most methods that assume a single constant illumination. Furthermore, capturing images under multiple illuminations

Submitted to the 37th Conference on Neural Information Processing Systems (NeurIPS 2023) Track on Datasets and Benchmarks. Do not distribute.

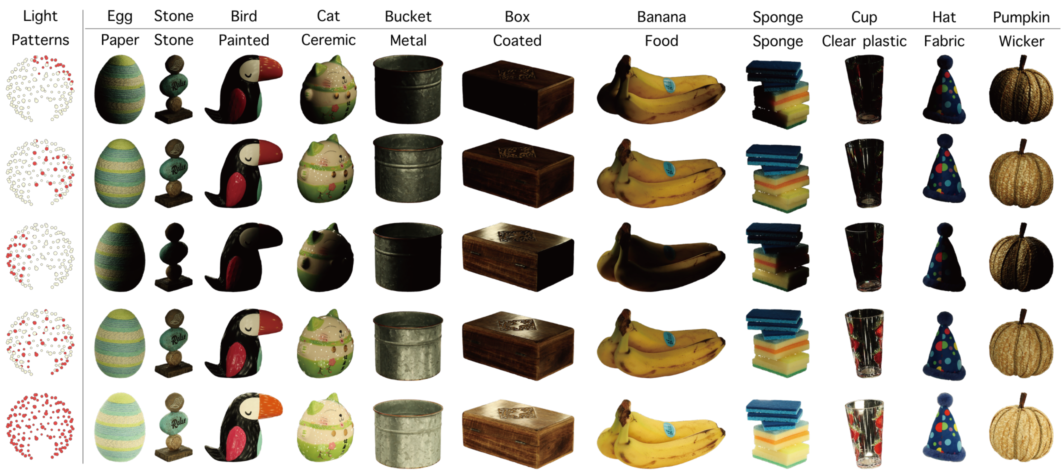

Figure 1: **Some example images in the proposed dataset.** The dataset contains images of various objects with diverse materials, captured under different views and illuminations. The leftmost column visualizes several different illumination patterns, with **red** and yellow indicating activated and deactivated lights. The name and material for each object are listed in the first and second rows. The materials are selected from the OpenSurfaces [3] dataset.

with a handheld camera often produces images with highly different appearances and results in inaccurate and even fail camera pose estimation, particularly for feature matching-based methods such as COLMAP [37]. Recent efforts have introduced some datasets [33, 43, 21] that incorporate multiple illuminations in real-world settings. However, as shown in Tab. 1, most of them are limited either in the number of views [33, 21] or the number of illuminations [21]; few of them provide object-level data as well. Consequently, these existing datasets prove unsuitable for evaluating inverse rendering methods on real-world objects.

To address this, we present a new dataset containing objects with a variety of materials, captured under multiple views and illuminations, allowing for reliable evaluation of various inverse rendering tasks with real data. Our dataset was acquired using a setup similar to a traditional light stage [10, 11], where densely distributed cameras and controllable lights are attached to a static frame around a central platform. In contrast to handheld capture, this setup allows us to precisely pre-calibrate all cameras with carefully designed calibration patterns and reuse the same camera parameters for all the target objects, leading to not only high calibration accuracy but also a consistent evaluation process (with the same camera parameters) for all the scenes.

On the other hand, the equipped multiple controllable lights enable us to flexibly illuminate objects with a large number of complex lighting patterns, facilitating the acquisition of illumination ground truth.

With the help of high-speed cameras running at 30 fps, we are able to capture OLAT (One-Light-At-a-Time) images with a very high efficiency, which is critical for capturing data at a large scale. In the end, we have captured over 108K images, each with a well-calibrated camera and illumination parameters. Moreover, we also provide high-quality object segmentation masks by designing an efficient semi-automatic mask labeling method.

We conduct baseline experiments on several tasks: (1) joint geometry-material-illumination estimation; (2) joint geometry-material estimation under known illumination; (3) photometric stereo reconstruction; (4) Novel view synthesis to showcase the ability to evaluating for real objects on our dataset. To the best of our knowledge, by the time of this paper's submission, there are no other real datasets that can be used to perform the quantitative evaluation for relighting on real data.

In summary, our contributions are as follows:

Dataset	Capturing device	Lighting condition	Number of illuminations	HDR	Number of scenes/objects	Number of views
DTU [19]	gantry	pattern	7	✗	80 scenes	49/64
NeRF-OSR [36]	commodity camera	env	5∼11	✗	9 scenes	∼360
DiLiGenT [39]	commodity camera	OLAT	96	✓	10 objects	1
DiLiGenT-MV [26]	studio/desktop scanner	OLAT	96	✓	5 objects	20
NeROIC [23]	commodity camera	env	4∼6	✗	3 objects	40
MIT-Intrinsic [15]	commodity camera	OLAT	10	✗	20 objects	1
Murmann et al. [33]	light probe	env	25	✗	1000 scenes	1
LSMI [21]	light probe	env	3	✗	2700 scenes	1
ReNe [43]	gantry	OLAT	40	✗	20 objects	50
Ours	light stage	pattern+OLAT	13 pattern+ 142 OLAT	✓	64 objects	72

Table 1: **Comparison between representative multi-illumination real-world datasets.** Env. stands for environment lights.

- We capture over 108K images for real objects with diverse materials under multiple viewpoints and illuminations, which enables a more comprehensive analysis for inverse rendering tasks across various material types.
- The proposed dataset provides precise camera calibrations, lighting ground truth and accurate object segmentation masks.
- We evaluate and compare the performance of multiple state-of-the-art (SOTA) inverse rendering and novel view synthesis methods. We perform quantitive evaluation of relighting real object under unseen illuminations.

2 Related works

Inverse rendering. Inverse rendering has been a long-standing task in the fields of computer vision and graphics, which focuses on reconstructing shapes and materials from multi-view 2D images. A great amount of work [5, 14, 18, 25, 47, 34, 52, 54] has been proposed for this task. Some of them make use of learned domain-specific priors [5, 12, 2, 27]. Some other works rely on controllable capture settings to estimate the geometry and material, such as structure light [48], circular LED lights [55], collocated camera and flashlight [50, 5, 4], and so on.

Recently, a lot of works use neural representations to support inverse rendering reconstruction under unknown natural lighting conditions [20, 6, 52, 54, 7, 32, 51]. By combining the popular neural representations such as NeRF [30] or SDF [45, 49] with physically-based rendering model [8], they can achieve shape and reflectance reconstruction with image loss constrain. Although these works can achieve high-quality reconstruction, they can only evaluate relighting performance under novel illumination on synthetic data because of the lack of high-quality real object datasets.

Multi-illumination datasets. Multi-illumination observations intuitively provide more cues for computer vision and graphics tasks like inverse rendering. Some works have utilized the temporal variation of natural illumination, such as sunlight and outdoor lighting. These "in-the-wild" images are typically captured using web cameras [46, 41, 36] or using controlled camera setups [40, 24]. Another line of works focuses on indoor scenes, while indoor scenes generally lack a readily-available source of illumination that exhibit significant variation. In this case, a common approach involves using flash and no-flash pairs [35, 13, 1]. Applications like denoising, mixed-lighting white balance, and BRDF capture benefits from these kinds of datasets. However, other applications like photometric stereo and inverse rendering usually require more than two images and more lighting conditions for reliable results, which these datasets often fail to provide.

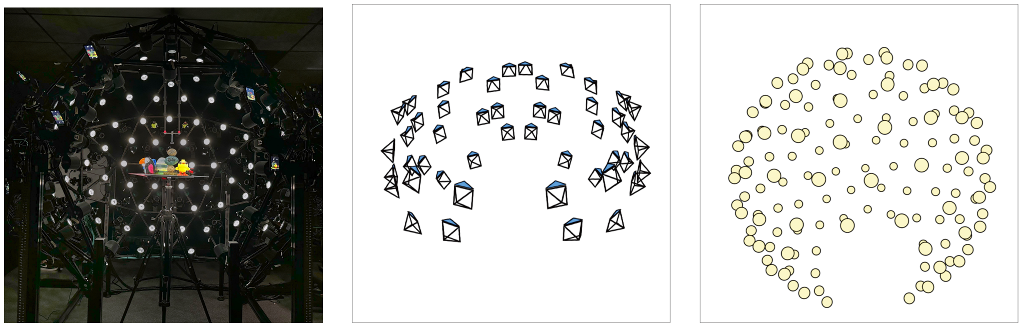

(a) (b) (c)

Figure 2: (a) The capturing system contains 48 DSLR cameras (Canon EOS Rebel SL3), 24 high-speed cameras (HR-12000SC), and 142 controllable linear polarized LED. (b) The calibrated DSLR camera poses. (c) The reconstructed light positions.

3 Dataset construction

3.1 Dataset overview

The OpenIllumination dataset contains over 108K images of 64 objects with diverse materials. Each object is captured by 48 DSLR cameras under 13 lighting patterns. Additionally, 20 objects are captured by 24 high-speed cameras under 142 OLAT setting.

Fig. 1 shows some images captured under different lighting patterns, while the images captured under OLAT illumination can be found in Fig. 5.

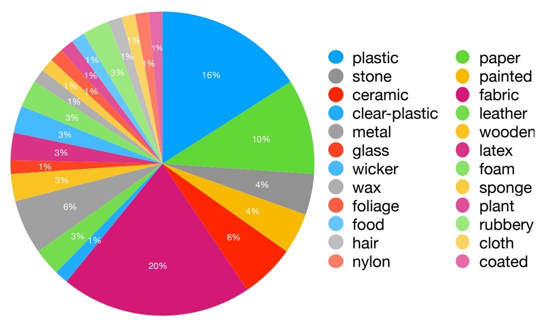

Our dataset includes a total of 24 diverse material categories, such as plastic, glass, fabric, ceramic, and more. Note that one object may possess several different materials, thus the number of materials is larger than the number of objects.

3.2 Camera calibration

The accuracy of camera calibration highly affects the performance of most novel view synthesis and inverse rendering methods. Previous works [20, 53] typically capture images by handheld cameras and employ COLMAP [37] to estimate camera parameters. However, this approach heavily relies on the object's textural properties, which is challenging in instances where the object lacks texture or exhibits specular reflections from certain viewpoints. These challenges can obstruct accurate feature matching, consequently reducing the precision of camera parameter estimation. Ultimately, the reliability of inverse rendering outcomes is undermined, and finding out whether inaccuracies are caused by erroneous camera parameters or limitations of the inverse rendering method itself becomes a challenging problem. Leveraging the capabilities of our light stage, wherein camera intrinsics and extrinsic can be fixed when capturing different objects, we employ COLMAP to recover the camera parameters on a textured and low-specularity scene. For each subsequently captured object, we use this set of camera parameters instead of performing recalibration. The results of camera calibration are visualized in Fig. 2(b).

3.3 Light calibration

In this section, we propose a chrome-ball-based lighting calibration method to obtain the ground-truth illumination which plays a critical role in the relighting evaluation.

Our data are captured in a dark room where a set of linear polarized LEDs are placed on a sphere uniformly as the only outer lighting source. Each light can be approximated by a Spherical Gaussian (SG), defined as the following form [44]:

$$G(\nu; \boldsymbol{\xi}, \lambda, \boldsymbol{\mu}) = \boldsymbol{\mu}\, e^{\lambda(\nu\cdot\boldsymbol{\xi}-1)}, \tag{1}$$

where $\nu \in \mathbb{S}^2$ is the function input, representing the incident lighting direction to query, $\boldsymbol{\xi} \in \mathbb{S}^2$ is the lobe axis, $\lambda \in \mathbb{R}_+$ is the lobe sharpness, and $\boldsymbol{\mu} \in \mathbb{R}^n_+$ is the lobe amplitude.

We utilize a chrome ball to estimate the 3D position of each light. Assuming the chrome ball is highly specular and isotropic, its position and radius are known, and cameras and lights are evenly distributed around the chrome ball. For each LED single light, at least one camera can capture the reflected light rays out from its starting location. The incident light direction can be computed via:

$$I = -T + 2(I \cdot N)N, \tag{2}$$

where I is the incident light direction that goes out from the point of incidence, N is the normal of the intersection point on the surface, and T is the direction of the reflected light.

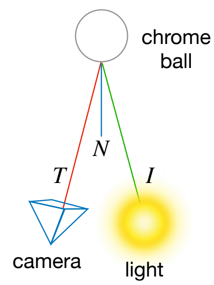

For each LED light, its point of incidence on the chrome ball can be captured by multiple cameras, and for each camera i, we can compute an incident light direction I_i, which should have the least distance from the LED light location p. Therefore, to leverage information from multiple camera viewpoints, we seek to minimize the sum of distances between the light position and incident light directions across different camera views. This optimization is expressed as:

$$L(p) = \sum_i d(p, I_i), \|p\| = 1, \tag{3}$$

where p represents the light position to be determined, $d(p, I_i)$ denotes the L2 distance between the light and the incident light direction corresponding to view i, and the constraint $\|p\| = 1$ ensures that the lights lie on the same spherical surface as the cameras. The reconstructed light distribution, depicted in Fig. 2(c), closely aligns with the real-world distribution.

After estimating the 3D position for each light, we need to determine lobe size for them. Since the lights in our setup are of the same type, we can estimate a global lobe size for all lights. By taking one OLAT image of the chrome ball as input, we flatten it into an environment map. Subsequently, we optimize the parameters of the Spherical Gaussians (SGs) model to minimize the difference between the computed environment map and the observed environment map.

Since all the lights have identical lighting intensities, and the lighting intensity can be of arbitrary scale because of the scale ambiguity between the material and lighting, we set the lighting intensity to 5 for all lights.

3.4 Semi-automatic high-quality mask labeling

To obtain high-quality segmentation masks, we use Segment-Anything [22] (SAM) to perform instance segmentation. However, we find that the performance is not satisfactory. One reason is that the object categories are highly undefined. In this case, even combining the bounding box and point prompts cannot produce satisfactory results. To address this problem, we use multiple bounding-box prompts to perform segmentation for each possible part and then calculate a union of the masks as the final object mask. For objects with very detailed and thin structures, e.g. hair, we use an off-the-shelf background matting method [28] to perform object segmentation.

4 Baseline experiments

4.1 Inverse rendering evaluation

In this section, we conduct experiments employing various learning-based inverse rendering methods on our dataset. Throughout these experiments, we carefully select 10 objects exhibiting a diverse

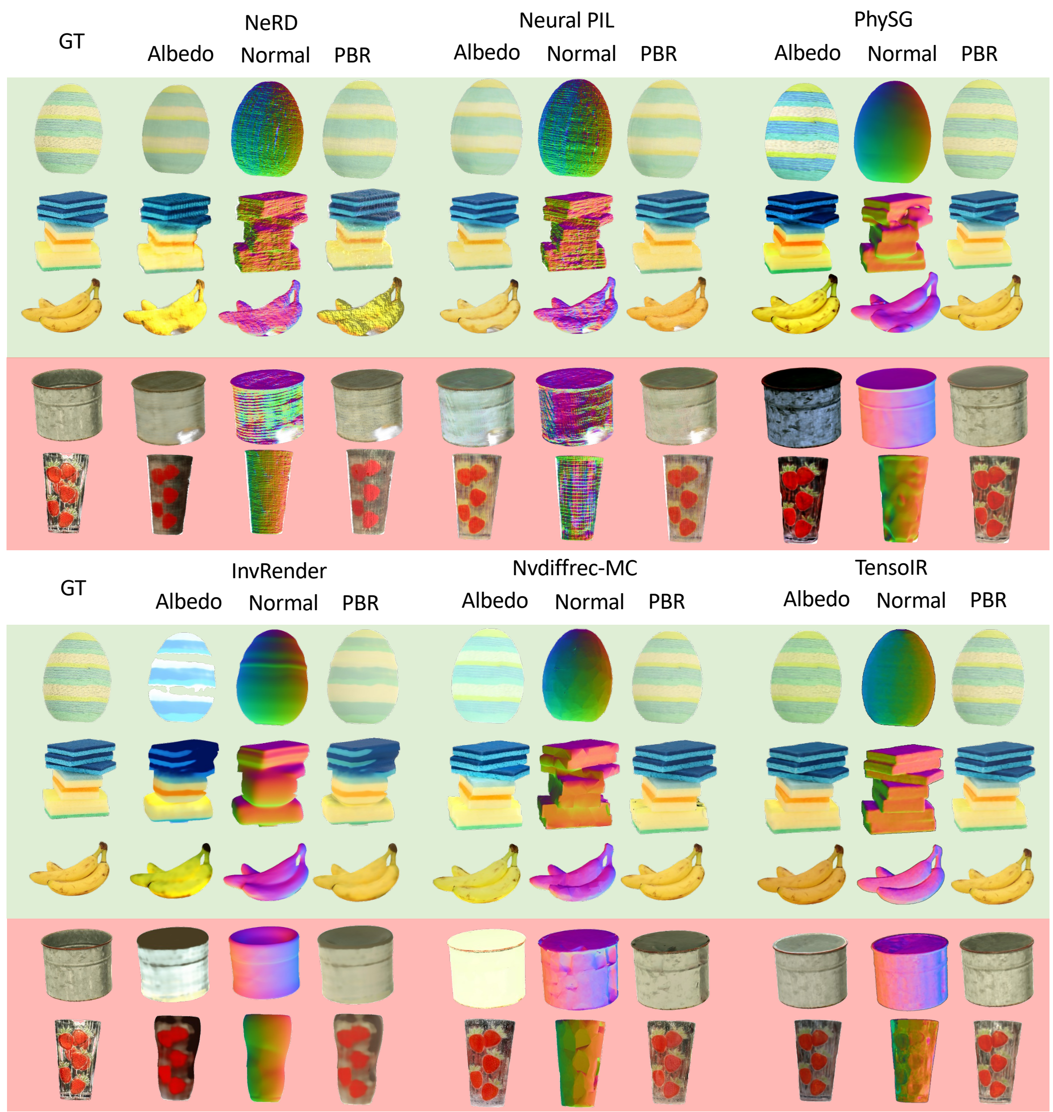

Figure 3: The object reconstruction on our dataset from three inverse rendering baselines under single illumination. Objects highlighted by **green** color are easier tasks in our dataset, while objects in **red** color are more difficult tasks that involve more complicated materials like metal and clear plastic.

range of materials, and we partition the images captured by DSLR cameras into training and testing sets, containing 38 and 10 views respectively.

Baselines. We validate six recent learning-based inverse rendering approaches assuming single illumination conditions: NeRD [6], Neural-PIL [7], PhysSG [51], InvRender [54], nvdiffrec-mc [16], and TensoIR [20]. Moreover, we validate three of them [6, 7, 20] that support multiple illumination optimization.

Joint geometry-material-illumination estimation. For experiments under single illumination, we use images captured with all lights activated, while for multi-illumination, we select images taken under three different lighting patterns.

NeRD[6] is observed to exhibit high instability. In many cases, NeRD fails to learn a meaningful environment map. Neural-PIL [7] generates fine environment maps and produces high-quality renderings. However, the generated environment map incorporates the albedo of objects and fails to produce reasonable diffuse results in multi-illumination conditions. Both NeRD and Neural-PIL suffer from map fractures in roughness, normal, and albedo, providing visible circular cracks, which we attribute to the overfitting of the environment map, where certain colors become embedded within it. PhySG [51] applies specular BRDFs allowing for a better approximate evaluation of light transport. PhySG shows commendable results on metal and coated materials, simulating a few highlights. But its geometry learning was inaccurate, and it performed poorly in objects with multiple specular parts, failing to reproduce any prominent highlights. InvRender [54] models spacially-varying indirection illumination and the visibility of direct illumination. However, its reconstructed geometry tends to lack detail and be over-smooth on some objects. nvdiffrec-mc [16] incorporates Monte Carlo integration and a denoising module during rendering to achieve a more efficient and stable convergence in optimization. It achieves satisfactory relighting results on most objects. But the quality of geometry detail as shown in the reconstructed normal map is affected by the grid resolution of DMTet [38]. TensoIR [20] also exhibits satisfactory performance. However, it still encounters challenges in generating good results for highly specular surfaces, as shown in the fourth row in Fig. 3. Moreover, since TensoIR models materials using a simplified version of Disney BRDF [8], which fixes the F_0 in the fresnel term to be 0.04, its representation capabilities are limited, and certain materials such as metal and transparent plastic may not be accurately modeled, as illustrated in the fifth row in Fig. 3 and Tab. 2, where TensoIR only achieve about 22 PSNR on the translucent plastic cup.

Overall, all the methods struggle with modeling transparency or complex reflectance because of the relatively simple BRDF used in rendering. For concave objects, such as the metal bucket shown in Fig. 3, NeRF-based methods have difficulty learning the correct geometry. In addition, compared to single illumination, two of our baselines, NeRD and NeuralPIL show inferior performance under multi-illumination, and the baseline TensoIR maintains a high quality of the reconstruction.

Object	egg	stone	bird	box	pumpkin	hat	cup	sponge	banana	bucket
Material	paper	stone	painted	coated	wooden	fabric	clear plastic	sponge	food	metal
NeRD	33.40	27.20	26.81	22.80	23.81	27.64	22.06	26.78	25.54	26.14
Neural-PIL	34.42	29.41	29.17	25.49	27.59	30.14	22.55	31.01	31.61	27.73
PhySG	35.06	30.72	29.02	26.56	27.32	31.16	21.86	30.70	34.39	29.25
InvRender	31.52	25.51	24.96	23.80	25.43	22.79	21.62	24.20	29.34	26.18
nvdiffrec-mc	35.77	31.51	30.20	27.29	28.12	31.19	22.08	32.68	35.60	28.52
TensoIR	34.88	29.96	30.21	26.80	28.20	31.96	22.13	32.49	34.77	29.32

Table 2: **Inverse rendering evaluation results under single illumination.** We validate six inverse rendering baselines with static illumination. We report the PSNR results for each object.

Object	egg	stone	bird	box	pumpkin	hat	cup	sponge	banana	bucket
Material	paper	stone	painted	coated	wooden	fabric	clear plastic	sponge	food	metal
NeRD	26.32	24.20	24.34	21.05	18.74	23.14	21.59	17.73	21.22	16.48
Neural-PIL	30.84	28.48	28.47	25.45	25.74	29.80	**22.44**	29.41	30.59	26.06
TensoIR	**34.51**	**29.88**	**30.21**	**26.53**	**27.96**	**31.58**	22.09	**31.87**	**34.35**	**28.91**

Table 3: **Inverse rendering evaluation results under multi-illumination.** We select three light patterns from our dataset to validate three baselines that support multiple illuminations. We report the PSNR results for each object.

Joint geometry-material estimation under known illumination. As introduced in Sec. 3.1, we capture the objects under different illuminations. For each illumination, we provide illumination ground truth represented as a combination of Spherical Gaussian functions. This enables us to evaluate the performance of relighting under novel illumination with the decomposed material and geometry.

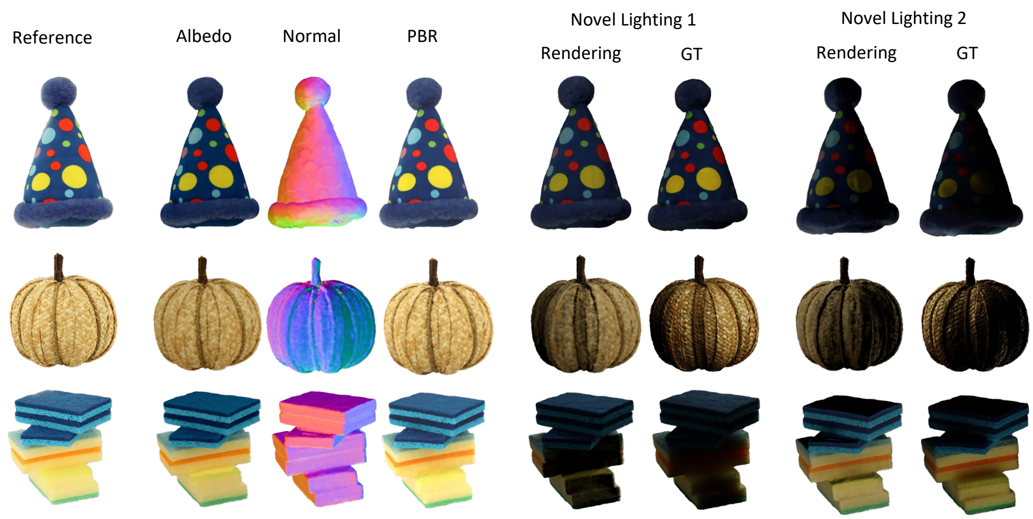

Figure 4: Relighting results of TensoIR under novel illumination. We show the reconstructed albedo, normal, and PBR results. For each novel illumination, we show the rendering and ground-truth captured images.

Object	egg	stone	bird	box	pumpkin	hat	cup	sponge	banana	bucket
Material	paper	stone	painted	coated	wooden	fabric	clear plastic	sponge	food	metal
PSNR	31.99	31.07	30.16	27.57	27.16	32.38	22.96	30.86	32.13	27.13

Table 4: Performance of relighting under novel illumination using TensoIR.

Tab. 4 shows the relighting performance of TensoIR [20] on 10 objects. Fig. 4 shows the material decomposition and the relighting visualizations. In general, TensoIR performs better on diffuse objects than on metal and transparent objects.

4.2 Photometric stereo

Photometric stereo (PS) is a well-established technique to reconstruct a 3D surface of an object [18]. The method estimates the shape and recovers surface normals of a scene by utilizing several intensity images obtained under varying illumination conditions with an identical viewpoint [17, 42]. By default, PS assumes a Lambertian surface reflectance, in which normal vectors and image intensities are linearly dependent on each other. During our capturing, we place circular polarizers over each light source, we also place a circular polarizer of the same sense in front of the camera to cancel out the specular reflections [29]. Fig. 5 shows the reconstructed albedo and normal map from the OLAT images in our dataset.

4.3 Novel view synthesis

Object	egg	stone	bird	box	pumpkin	hat	cup	sponge	banana	bucket
Material	paper	stone	painted	coated	wooden	fabric	clear plastic	sponge	food	metal
NeRF [30]	33.53	29.32	29.64	25.38	26.95	31.29	**22.52**	31.36	33.65	28.54
TensoRF [9]	32.42	29.84	28.45	**25.49**	27.54	31.50	20.87	31.34	34.32	29.28
I-NGP [31]	**34.07**	**30.62**	29.91	25.83	**27.93**	**32.51**	22.51	**32.71**	**34.98**	29.72
NeuS [45]	33.43	29.78	**30.00**	25.47	27.83	31.93	22.13	32.44	34.17	**29.99**

Table 5: **Novel-view-synthesis PSNR on NeRF, TensoRF, Instant-NGP, and NeuS.**

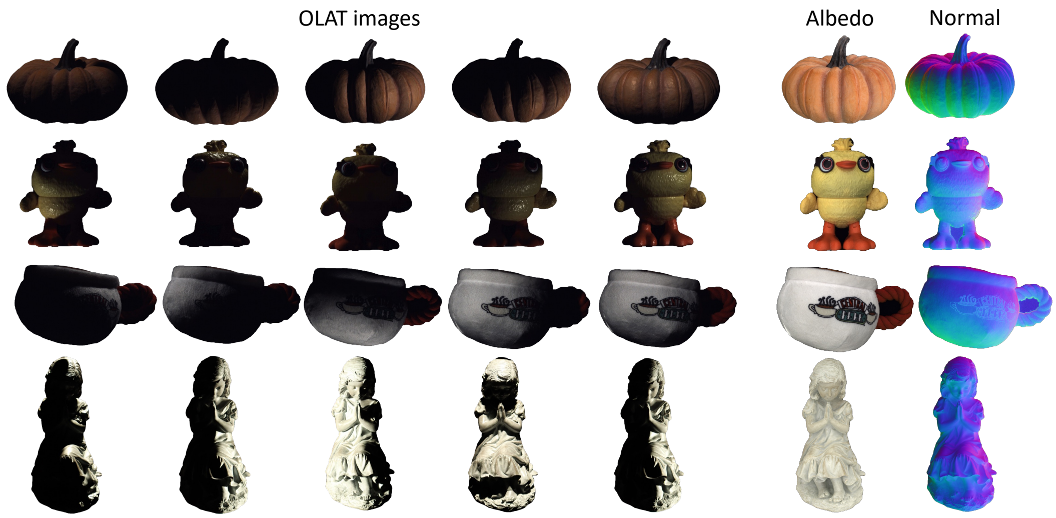

Figure 5: Results of photometric stereo using the OLAT images in our dataset.

While our dataset was primarily proposed for evaluating inverse rendering approaches, the multi-view images in it can also serve as a valuable resource for evaluating novel view synthesis methods. In this section, we perform experiments utilizing several neural radiance field methods to validate the data quality of our dataset. We conduct experiments employing the vanilla NeRF [30], TensoRF [9], Instant-NGP [31], and NeuS [45]. The quantitative results, as presented in Tab. 5, demonstrate the exceptional quality of our data and the precise camera calibration, as evidenced by the consistently high PSNR scores attained.

4.4 Ablation study

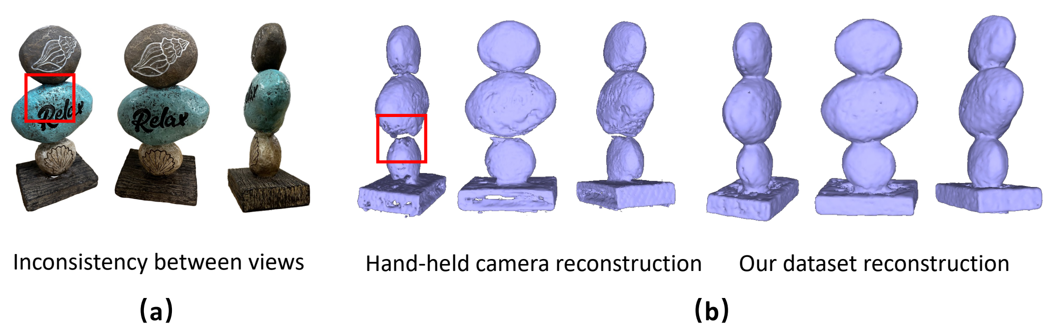

Figure 6: **(a)** Capturing using a handheld camera often introduces inconsistent illuminations. **(b)** Geometry reconstruction using data in our dataset delivers higher completion than using data captured by handheld cameras.

As depicted in Fig. 6(a), the utilization of handheld cameras in the capture process frequently gives rise to inconsistent illumination between different viewpoints because of the changing occlusion of light caused by the moving photographer, thereby breaching the static illumination assumption for most inverse rendering methods. Furthermore, using handheld cameras tends to inadequately ensure an extensive range of viewpoints, thereby frequently resulting in the incompleteness of the reconstructed objects. Conversely, our dataset delivers a superior range of viewpoints and maintains consistency across different objects, thereby producing a more complete reconstruction. This demonstrates the high quality of our dataset and establishes its suitability as an evaluation benchmark for real-world objects.

5 Limitation

There are several limitations and future directions to our work. **(1)** Since we use the light stage to capture the images in a dark room, the illumination is controlled strictly. Thus there exists a gap between the images in this dataset and in-the-wild captured images. **(2)** Although we use state-of-the-art methods for segmentation, the mask consistency across different views for smaller objects with fine details, such as hair, is not considered yet. **(3)** Due to the limited space, the sizes of the objects in the dataset are restricted to 10$\sim$20 cm, and the cameras are not highly densely distributed.

6 Conclusion

In this paper, we introduce a multi-illumination dataset OpenIllumination for inverse rendering evaluation on real objects. This dataset offers crucial components such as precise camera parameters, ground-truth illumination information, and segmentation masks for all the images. OpenIllumination provides a valuable resource for quantitatively evaluating inverse rendering and material decomposition techniques applied to real objects for researchers. By analyzing various state-of-the-art inverse rendering pipelines using our dataset, we have been able to assess and compare their performance effectively. The release of both the dataset and accompanying code will be made available, encouraging further exploration and advancement in this field.

References

[1] Yagiz Aksoy, Changil Kim, Petr Kellnhofer, Sylvain Paris, Mohamed Elgharib, Marc Pollefeys, and Wojciech Matusik. A dataset of flash and ambient illumination pairs from the crowd. In *Proceedings of the European Conference on Computer Vision (ECCV)*, pages 634–649, 2018.

[2] Jonathan T Barron and Jitendra Malik. Shape, illumination, and reflectance from shading. *IEEE transactions on pattern analysis and machine intelligence*, 37(8):1670–1687, 2015.

[3] Sean Bell, Paul Upchurch, Noah Snavely, and Kavita Bala. Opensurfaces: A richly annotated catalog of surface appearance. *ACM Transactions on graphics (TOG)*, 32(4):1–17, 2013.

[4] Sai Bi, Zexiang Xu, Pratul P. Srinivasan, Ben Mildenhall, Kalyan Sunkavalli, Milovs Havsan, Yannick Hold-Geoffroy, David J. Kriegman, and Ravi Ramamoorthi. Neural reflectance fields for appearance acquisition. *ArXiv*, abs/2008.03824, 2020.

[5] Sai Bi, Zexiang Xu, Kalyan Sunkavalli, David Kriegman, and Ravi Ramamoorthi. Deep 3d capture: Geometry and reflectance from sparse multi-view images. In *Proceedings of the IEEE/CVF Conference on Computer Vision and Pattern Recognition*, pages 5960–5969, 2020.

[6] Mark Boss, Raphael Braun, Varun Jampani, Jonathan T Barron, Ce Liu, and Hendrik Lensch. Nerd: Neural reflectance decomposition from image collections. In *Proceedings of the IEEE/CVF International Conference on Computer Vision*, pages 12684–12694, 2021.

[7] Mark Boss, Varun Jampani, Raphael Braun, Ce Liu, Jonathan Barron, and Hendrik Lensch. Neural-pil: Neural pre-integrated lighting for reflectance decomposition. *Advances in Neural Information Processing Systems*, 34:10691–10704, 2021.

[8] Brent Burley and Walt Disney Animation Studios. Physically-based shading at disney. In *ACM SIGGRAPH*, volume 2012, pages 1–7. vol. 2012, 2012.

[9] Anpei Chen, Zexiang Xu, Andreas Geiger, Jingyi Yu, and Hao Su. Tensorf: Tensorial radiance fields. In *Computer Vision–ECCV 2022: 17th European Conference, Tel Aviv, Israel, October 23–27, 2022, Proceedings, Part XXXII*, pages 333–350. Springer, 2022.

[10] Paul Debevec, Tim Hawkins, Chris Tchou, Haarm-Pieter Duiker, Westley Sarokin, and Mark Sagar. Acquiring the reflectance field of a human face. In *Proceedings of the 27th annual conference on Computer graphics and interactive techniques*, pages 145–156, 2000.

[11] Paul Debevec, Andreas Wenger, Chris Tchou, Andrew Gardner, Jamie Waese, and Tim Hawkins. A lighting reproduction approach to live-action compositing. *ACM Transactions on Graphics (TOG)*, 21(3):547–556, 2002.

[12] Yue Dong, Guojun Chen, Pieter Peers, Jiawan Zhang, and Xin Tong. Appearance-from-motion: Recovering spatially varying surface reflectance under unknown lighting. *ACM Transactions on Graphics*, 33(6):193, 2014.

[13] Elmar Eisemann and Frédo Durand. Flash photography enhancement via intrinsic relighting. *ACM transactions on graphics (TOG)*, 23(3):673–678, 2004.

[14] Dan B Goldman, Brian Curless, Aaron Hertzmann, and Steven M Seitz. Shape and spatially-varying brdfs from photometric stereo. *IEEE Transactions on Pattern Analysis and Machine Intelligence*, 32(6):1060–1071, 2009.

[15] Roger Grosse, Micah K Johnson, Edward H Adelson, and William T Freeman. Ground truth dataset and baseline evaluations for intrinsic image algorithms. In *2009 IEEE 12th International Conference on Computer Vision*, pages 2335–2342. IEEE, 2009.

[16] Jon Hasselgren, Nikolai Hofmann, and Jacob Munkberg. Shape, light & material decomposition from images using monte carlo rendering and denoising. *arXiv preprint arXiv:2206.03380*, 2022.

[17] Hideki Hayakawa. Photometric stereo under a light source with arbitrary motion. *JOSA A*, 11(11):3079–3089, 1994.

[18] Carlos Hernandez, George Vogiatzis, and Roberto Cipolla. Multiview photometric stereo. *IEEE Transactions on Pattern Analysis and Machine Intelligence*, 30(3):548–554, 2008.

[19] Rasmus Jensen, Anders Dahl, George Vogiatzis, Engin Tola, and Henrik Aanæs. Large scale multi-view stereopsis evaluation. In *Proceedings of the IEEE conference on computer vision and pattern recognition*, pages 406–413, 2014.

[20] Haian Jin, Isabella Liu, Peijia Xu, Xiaoshuai Zhang, Songfang Han, Sai Bi, Xiaowei Zhou, Zexiang Xu, and Hao Su. Tensoir: Tensorial inverse rendering. In *Proceedings of the IEEE/CVF Conference on Computer Vision and Pattern Recognition*, pages 165–174, 2023.

[21] Dongyoung Kim, Jinwoo Kim, Seonghyeon Nam, Dongwoo Lee, Yeonkyung Lee, Nahyup Kang, Hyong-Euk Lee, ByungIn Yoo, Jae-Joon Han, and Seon Joo Kim. Large scale multi-illuminant (lsmi) dataset for developing white balance algorithm under mixed illumination. In *Proceedings of the IEEE/CVF International Conference on Computer Vision*, pages 2410–2419, 2021.

[22] Alexander Kirillov, Eric Mintun, Nikhila Ravi, Hanzi Mao, Chloe Rolland, Laura Gustafson, Tete Xiao, Spencer Whitehead, Alexander C Berg, Wan-Yen Lo, et al. Segment anything. *arXiv preprint arXiv:2304.02643*, 2023.

[23] Zhengfei Kuang, Kyle Olszewski, Menglei Chai, Zeng Huang, Panos Achlioptas, and Sergey Tulyakov. Neroic: Neural rendering of objects from online image collections. *ACM Transactions on Graphics (TOG)*, 41(4):1–12, 2022.

[24] Jean-François Lalonde and Iain Matthews. Lighting estimation in outdoor image collections. In *2014 2nd international conference on 3D vision*, volume 1, pages 131–138. IEEE, 2014.

[25] Jason Lawrence, Szymon Rusinkiewicz, and Ravi Ramamoorthi. Efficient brdf importance sampling using a factored representation. *ACM Transactions on Graphics (ToG)*, 23(3):496–505, 2004.

[26] Min Li, Zhenglong Zhou, Zhe Wu, Boxin Shi, Changyu Diao, and Ping Tan. Multi-view photometric stereo: A robust solution and benchmark dataset for spatially varying isotropic materials. *IEEE Transactions on Image Processing*, 29:4159–4173, 2020.

[27] Zhengqin Li, Zexiang Xu, Ravi Ramamoorthi, Kalyan Sunkavalli, and Manmohan Chandraker. Learning to reconstruct shape and spatially-varying reflectance from a single image. In *SIGGRAPH Asia 2018*, page 269. ACM, 2018.

[28] Shanchuan Lin, Andrey Ryabtsev, Soumyadip Sengupta, Brian L Curless, Steven M Seitz, and Ira Kemelmacher-Shlizerman. Real-time high-resolution background matting. In *Proceedings of the IEEE/CVF Conference on Computer Vision and Pattern Recognition*, pages 8762–8771, 2021.

[29] Wan-Chun Ma, Tim Hawkins, Pieter Peers, Charles-Felix Chabert, Malte Weiss, Paul E Debevec, et al. Rapid acquisition of specular and diffuse normal maps from polarized spherical gradient illumination. *Rendering Techniques*, 2007(9):10, 2007.

[30] Ben Mildenhall, Pratul P Srinivasan, Matthew Tancik, Jonathan T Barron, Ravi Ramamoorthi, and Ren Ng. Nerf: Representing scenes as neural radiance fields for view synthesis. *Communications of the ACM*, 65(1):99–106, 2021.

[31] Thomas Müller, Alex Evans, Christoph Schied, and Alexander Keller. Instant neural graphics primitives with a multiresolution hash encoding. *ACM Transactions on Graphics (ToG)*, 41(4):1–

15, 2022.

[32] Jacob Munkberg, Jon Hasselgren, Tianchang Shen, Jun Gao, Wenzheng Chen, Alex Evans, Thomas Mueller, and Sanja Fidler. Extracting Triangular 3D Models, Materials, and Lighting From Images. *arXiv:2111.12503*, 2021.

[33] Lukas Murmann, Michael Gharbi, Miika Aittala, and Fredo Durand. A dataset of multi-illumination images in the wild. In *Proceedings of the IEEE/CVF International Conference on Computer Vision*, pages 4080–4089, 2019.

[34] Giljoo Nam, Joo Ho Lee, Diego Gutierrez, and Min H Kim. Practical SVBRDF acquisition of 3D objects with unstructured flash photography. In *SIGGRAPH Asia 2018*, page 267. ACM, 2018.

[35] Georg Petschnigg, Richard Szeliski, Maneesh Agrawala, Michael Cohen, Hugues Hoppe, and Kentaro Toyama. Digital photography with flash and no-flash image pairs. *ACM transactions on graphics (TOG)*, 23(3):664–672, 2004.

[36] Viktor Rudnev, Mohamed Elgharib, William Smith, Lingjie Liu, Vladislav Golyanik, and Christian Theobalt. Nerf for outdoor scene relighting. In *European Conference on Computer Vision (ECCV)*, 2022.

[37] Johannes L Schönberger, Enliang Zheng, Jan-Michael Frahm, and Marc Pollefeys. Pixelwise view selection for unstructured multi-view stereo. In *Computer Vision–ECCV 2016: 14th European Conference, Amsterdam, The Netherlands, October 11-14, 2016, Proceedings, Part III 14*, pages 501–518. Springer, 2016.

[38] Tianchang Shen, Jun Gao, Kangxue Yin, Ming-Yu Liu, and Sanja Fidler. Deep marching tetrahedra: a hybrid representation for high-resolution 3d shape synthesis. In *Advances in Neural Information Processing Systems (NeurIPS)*, 2021.

[39] Boxin Shi, Zhe Wu, Zhipeng Mo, Dinglong Duan, Sai-Kit Yeung, and Ping Tan. A benchmark dataset and evaluation for non-lambertian and uncalibrated photometric stereo. In *Proceedings of the IEEE Conference on Computer Vision and Pattern Recognition*, pages 3707–3716, 2016.

[40] Jessi Stumpfel, Andrew Jones, Andreas Wenger, Chris Tchou, Tim Hawkins, and Paul Debevec. Direct hdr capture of the sun and sky. In *ACM SIGGRAPH 2006 Courses*, pages 5–es. 2006.

[41] Kalyan Sunkavalli, Fabiano Romeiro, Wojciech Matusik, Todd Zickler, and Hanspeter Pfister. What do color changes reveal about an outdoor scene? In *2008 IEEE Conference on Computer Vision and Pattern Recognition*, pages 1–8. IEEE, 2008.

[42] Ariel Tankus and Nahum Kiryati. Photometric stereo under perspective projection. In *Tenth IEEE International Conference on Computer Vision (ICCV'05) Volume 1*, volume 1, pages 611–616. IEEE, 2005.

[43] Marco Toschi, Riccardo De Matteo, Riccardo Spezialetti, Daniele De Gregorio, Luigi Di Stefano, and Samuele Salti. Relight my nerf: A dataset for novel view synthesis and relighting of real world objects. In *Proceedings of the IEEE/CVF Conference on Computer Vision and Pattern Recognition*, pages 20762–20772, 2023.

[44] Jiaping Wang, Peiran Ren, Minmin Gong, John Snyder, and Baining Guo. All-frequency rendering of dynamic, spatially-varying reflectance. In *ACM SIGGRAPH Asia 2009 papers*, pages 1–10. 2009.

[45] Peng Wang, Lingjie Liu, Yuan Liu, Christian Theobalt, Taku Komura, and Wenping Wang. Neus: Learning neural implicit surfaces by volume rendering for multi-view reconstruction. *arXiv preprint arXiv:2106.10689*, 2021.

[46] Yair Weiss. Deriving intrinsic images from image sequences. In *Proceedings Eighth IEEE International Conference on Computer Vision. ICCV 2001*, volume 2, pages 68–75. IEEE, 2001.

[47] Rui Xia, Yue Dong, Pieter Peers, and Xin Tong. Recovering shape and spatially-varying surface reflectance under unknown illumination. *ACM Transactions on Graphics*, 35(6):187, 2016.

[48] Xianmin Xu, Yuxin Lin, Haoyang Zhou, Chong Zeng, Yaxin Yu, Kun Zhou, and Hongzhi Wu. A unified spatial-angular structured light for single-view acquisition of shape and reflectance. In *Proceedings of the IEEE/CVF Conference on Computer Vision and Pattern Recognition*, pages 206–215, 2023.

[49] Lior Yariv, Yoni Kasten, Dror Moran, Meirav Galun, Matan Atzmon, Basri Ronen, and Yaron Lipman. Multiview neural surface reconstruction by disentangling geometry and appearance. *Advances in Neural Information Processing Systems*, 33:2492–2502, 2020.

[50] Kai Zhang, Fujun Luan, Zhengqi Li, and Noah Snavely. Iron: Inverse rendering by optimizing neural sdfs and materials from photometric images. In *Proceedings of the IEEE/CVF Conference on Computer Vision and Pattern Recognition*, pages 5565–5574, 2022.

[51] Kai Zhang, Fujun Luan, Qianqian Wang, Kavita Bala, and Noah Snavely. Physg: Inverse rendering with spherical gaussians for physics-based material editing and relighting. In *Proceedings of the IEEE/CVF Conference on Computer Vision and Pattern Recognition*, pages 5453–5462, 2021.

[52] Xiuming Zhang, Pratul P Srinivasan, Boyang Deng, Paul Debevec, William T Freeman, and Jonathan T Barron. Nerfactor: Neural factorization of shape and reflectance under an unknown illumination. *ACM Transactions on Graphics (TOG)*, 40(6):1–18, 2021.

[53] Yuanqing Zhang, Jiaming Sun, Xingyi He, Huan Fu, Rongfei Jia, and Xiaowei Zhou. Modeling indirect illumination for inverse rendering. In *Proceedings of the IEEE/CVF Conference on Computer Vision and Pattern Recognition*, pages 18643–18652, 2022.

[54] Yuanqing Zhang, Jiaming Sun, Xingyi He, Huan Fu, Rongfei Jia, and Xiaowei Zhou. Modeling indirect illumination for inverse rendering. In *Proceedings of the IEEE/CVF Conference on Computer Vision and Pattern Recognition*, pages 18643–18652, 2022.

[55] Zhenglong Zhou, Zhe Wu, and Ping Tan. Multi-view photometric stereo with spatially varying isotropic materials. In *Proceedings of the IEEE Conference on Computer Vision and Pattern Recognition*, pages 1482–1489, 2013.

Checklist

1. For all authors...
   (a) Do the main claims made in the abstract and introduction accurately reflect the paper's contributions and scope? [Yes]
   (b) Did you describe the limitations of your work? [Yes]
   (c) Did you discuss any potential negative societal impacts of your work? [No] There are no negative societal impacts of our work.
   (d) Have you read the ethics review guidelines and ensured that your paper conforms to them? [Yes] We have read the ethics review guidelines and ensured that our paper conforms to them.
2. If you are including theoretical results...
   (a) Did you state the full set of assumptions of all theoretical results? [No] We didn't include theoretical results.
   (b) Did you include complete proofs of all theoretical results? [No] We didn't include theoretical results.
3. If you ran experiments (e.g. for benchmarks)...
   (a) Did you include the code, data, and instructions needed to reproduce the main experimental results (either in the supplemental material or as a URL)? [Yes] We have provided the URLs for the code in the supplementary material.
   (b) Did you specify all the training details (e.g., data splits, hyperparameters, how they were chosen)? [Yes] .We specify all the training details in Sec. 4. For inverse rendering and novel-view-synthesis experiments, the camera views are randomly split into training and testing views with 38 and 10 views for each object.
   (c) Did you report error bars (e.g., with respect to the random seed after running experiments multiple times)? [No] We didn't report error bars for the baseline experiments. The inverse rendering methods are typically very time-consuming. For example, NeRD takes 130 hours and 288 hours to train under single and multi-illumination settings for each object on a GTX 2080 GPU with 800 $\times$1200 resolution images as input, and Neural-PIL takes 44 and 78 hours. Given that we have many objects in our dataset, it is not practical to run the experiments multiple times.

(d) Did you include the total amount of compute and the type of resources used (e.g., type of GPUs, internal cluster, or cloud provider)? [Yes] We have mentioned that we used a single GTX 2080 GPU to run the baseline experiments for each object.

4. If you are using existing assets (e.g., code, data, models) or curating/releasing new assets...
   (a) If your work uses existing assets, did you cite the creators? [No] We did not use any existing assets.
   (b) Did you mention the license of the assets? [No] We did not use any existing assets.
   (c) Did you include any new assets either in the supplemental material or as a URL? [Yes] We have provided data URL in the supplemental material.
   (d) Did you discuss whether and how consent was obtained from people whose data you're using/curating? [No] We did not use any existing assets.
   (e) Did you discuss whether the data you are using/curating contains personally identifiable information or offensive content? [Yes] Our dataset does not contain any personally identifiable information or offensive content since the content are all objects.
5. If you used crowdsourcing or conducted research with human subjects...
   (a) Did you include the full text of instructions given to participants and screenshots, if applicable? [No] We didn't use crowdsourcing or conducted research with human subjects.
   (b) Did you describe any potential participant risks, with links to Institutional Review Board (IRB) approvals, if applicable? [No] We didn't use crowdsourcing or conducted research with human subjects.
   (c) Did you include the estimated hourly wage paid to participants and the total amount spent on participant compensation? [No] We didn't use crowdsourcing or conducted research with human subjects.